On the Influence of Orography on Large-Scale Atmospheric Flow

WILLIAM L. GROSE[1]

NASA Langley Research Center, Hampton, VA 23665

BRIAN J. HOSKINS

U.K. Universities' Atmospheric Modelling Group, Department of Meteorology, University of Reading, England

(Manuscript received 16 January 1978, in final form 27 October 1978)

ABSTRACT

An investigation has been conducted of the steady response to orography as described by the linearized shallow-water equations on the sphere. Results have been obtained for both idealized and realistic climatological mean zonal flows when perturbed by simple isolated mountains. The response is interpreted in terms of the Rossby wavetrains and the energy dispersion ideas developed in Hoskins *et al.* (1977). Subsequent results from perturbing the several zonal flows by the earth orography are then readily understood. The surprisingly good comparison with observation suggests that the qualitative insight gained from the simple model is useful. The main difference from previous work is the emphasis on the two-dimensional nature of the horizontal propagation on the sphere. In particular, for a jet at 30° impinging on a mountain at the same latitude, there is a tendency to produce two wavetrains—one to the north and one to the south. At 60°–80° downstream these wavetrains are out of phase, giving a "blocking" region with a ridge to the north and a trough to the south. The southern train produces enhanced equatorial easterlies centered 30°–40° downstream.

The results give interesting indications of the regions of influence of mountains and suggest that quantitative theories of the stationary waves must contain a full representation of the spherical domain.

1. Introduction

Since the pioneering work of Charney and Eliassen (1949), there have been numerous studies of the effects of large-scale orography on atmospheric flow. Using barotropic models, Charney and Eliassen (1949) and Bolin (1950) concluded that the large-scale stationary disturbances in the midlatitude westerlies are largely a result of orographic forcing. However, Smagorinsky (1953) and Gilchrist (1954) showed thermal forcing to have an important role. Subsequent studies have used more complicated models to consider the separate or combined effects of thermal and orographic forcing. Kasahara (1966) used the time-dependent shallow-water equations in a beta-plane channel and Egger (1976a) the steady, linear, two-level primitive equations on the hemisphere to study the role of orography. Derome and Wiin-Nielsen (1971) used a beta-plane quasi-geostrophic model to study the effect of the two forcings. Egger (1976b) conducted a similar study with his hemispheric two-level model and Manabe and Terpstra (1974) and Kasahara *et al.* (1973) used full general circulation models for this problem. The results of these and other papers have demonstrated the importance of both thermal and orographic forcing.

In an attempt to provide insight into the dynamical effects of large-scale orographic features on atmospheric motion, we now consider the steady response to orography as described by the shallow water equations on the sphere. The mountains and zonal flows used in this study vary from idealized to realistic representations. In Hoskins *et al.* (1977, hereinafter referred to as H), the propagation of energy and vorticity as described by the linearized, barotropic vorticity equation on the sphere was examined. In the present paper emphasis is placed on qualitative features associated with wave propagation, some of which may be understood using the ideas discussed in *H*, rather than on quantitative details for which the model is not appropriate. The importance of north–south propagation is again stressed.

Section 2 introduces the model equations and the zonal flows and orography used in the study. Most of the mathematical detail is contained in an Appendix. The results for simple mountains are given in Section 3, and for the earth orography in Section 4.

2. Description of the model equations, zonal flows and orography

a. Model equations

Using variables nondimensionalized by the planetary radius a_0 and angular velocity Ω, the shallow water

[1] Research performed while on leave of absence at the University of Reading.

0022-4928/79/020223-12$07.00

equations on the sphere may be written

$$\frac{\partial \zeta}{\partial t}=-\frac{1}{1-\mu^2}\frac{\partial}{\partial \lambda}(U\zeta)-\frac{\partial}{\partial \mu}(V\zeta), \tag{1}$$

$$\frac{\partial D}{\partial t}=\frac{1}{1-\mu^2}\frac{\partial}{\partial \lambda}(V\zeta)-\frac{\partial}{\partial \mu}(U\zeta)-\nabla^2\left[\frac{U^2+V^2}{2(1-\mu^2)}+\phi\right], \tag{2}$$

$$\frac{\partial \phi}{\partial t}=-\Phi D-\frac{1}{1-\mu^2}\frac{\partial}{\partial \lambda}[U(\phi-\phi^*)]-\frac{\partial}{\partial \mu}[V(\phi-\phi^*)], \tag{3}$$

where ζ is the absolute vorticity, D the divergence, Φ the average height of the fluid multiplied by the gravitational constant g, ϕ the deviation of the free surface from that height multiplied by g and ϕ^* the height of the orography multiplied by g. The latitude and longitude are denoted by θ and λ with $\mu=\sin\theta$. The variables U and V are the zonal and meridional velocities multiplied by $\cos\theta$.

A velocity potential α, streamfunction ψ and relative vorticity ξ may be introduced giving the internal relations

$$\zeta=\xi+2\mu, \tag{4}$$

$$\xi=\nabla^2\psi=\frac{1}{1-\mu^2}\frac{\partial V}{\partial \lambda}-\frac{\partial V}{\partial \mu}, \tag{5}$$

$$D=\nabla^2\alpha=\frac{1}{1-\mu^2}\frac{\partial U}{\partial \lambda}+\frac{\partial V}{\partial \mu}, \tag{6}$$

$$U=\frac{\partial \alpha}{\partial \lambda}-(1-\mu^2)\frac{\partial \psi}{\partial \mu}, \tag{7}$$

$$V=\frac{\partial \psi}{\partial \lambda}+(1-\mu^2)\frac{\partial \alpha}{\partial \mu}. \tag{8}$$

We shall look for steady solutions

$$U=\bar{U}(\mu)+U'(\lambda,\mu),$$
$$V=V'(\lambda,\mu),$$
$$\zeta=\bar{\zeta}(\mu)+\zeta'(\lambda,\mu),$$
$$\phi=\bar{\phi}(\mu)+\phi'(\lambda,\mu),$$

where the barred quantities refer to a specified zonal flow and the primed quantities denote small perturbations forced by the orography. In order that the zonal flow satisfy the governing equations, we require

$$\frac{\partial \bar{\phi}}{\partial \mu}=-\mu\left[\frac{2\bar{U}}{1-\mu^2}+\left(\frac{\bar{U}}{1-\mu^2}\right)^2\right]. \tag{9}$$

The linearized perturbation equations for ψ', α' and ϕ' from (1)–(8) may be written

$$\frac{\bar{U}}{1-\mu^2}\nabla^2\left(\frac{\partial \psi'}{\partial \lambda}\right)+\frac{\partial \bar{\zeta}}{\partial \mu}\left[\frac{\partial \psi'}{\partial \lambda}+(1-\mu^2)\frac{\partial \alpha'}{\partial \mu}\right]+\bar{\zeta}\nabla^2\alpha'=0, \tag{10}$$

$$\bar{U}\nabla^2\left(\frac{\partial \psi'}{\partial \mu}\right)+\frac{\partial \bar{\zeta}}{\partial \mu}\left[\frac{\partial \alpha'}{\partial \lambda}-(1-\mu^2)\frac{\partial \psi'}{\partial \mu}\right]-\nabla^2\psi'\left(\bar{\zeta}-\frac{\partial \bar{U}}{\partial \mu}\right)$$
$$+\nabla^2\left\{\frac{\bar{U}}{1-\mu^2}\left[\frac{\partial \alpha'}{\partial \lambda}-(1-\mu^2)\frac{\partial \psi'}{\partial \mu}\right]+\phi'\right\}=0, \tag{11}$$

$$\frac{\bar{U}}{1-\mu^2}\frac{\partial \phi'}{\partial \lambda}+\frac{\partial \bar{\phi}}{\partial \mu}\left[\frac{\partial \psi'}{\partial \lambda}+(1-\mu^2)\frac{\partial \alpha'}{\partial \mu}\right]$$
$$+\nabla^2\alpha'(\Phi+\bar{\phi})=\frac{\bar{U}}{1-\mu^2}\frac{\partial \phi^*}{\partial \lambda}. \tag{12}$$

As described in the Appendix, truncated spherical harmonic expansions are used for the dependent variables, and solutions may be obtained by matrix inversion. The truncation selected for this study is rhomboidal, retaining all zonal wavenumbers up to 32 and 32 degrees of freedom in the latitudinal direction for each zonal wavenumber.

Solutions were presented in H for a time-dependent problem where a vorticity source gave rise to a train of waves, the front of which propagates around the sphere in typically 20 days. After this time, depending on the phase of the wave, there was the possibility of reinforcement and large amplitudes. In a steady problem, this phenomenom of resonance may lead to great sensitivity of the solutions. Following Charney and Eliassen (1949), we include a linear drag term which is sufficient to damp the waves in less than 20 days, and thus remove the sensitivity implied by resonance. The drag coefficient K used gives an e-folding time for damping of 14.7 days and is the medium value used by Charney and Eliassen (1949). A test experiment using double the drag confirmed the lack of sensitivity of our results to this rather arbitrary coefficient. A further complication is that extremely strong gradients may be expected near a critical line at which the zonal flow velocity is zero. For this reason, a biharmonic (∇^4) horizontal diffusion is also included. The coefficient K' is the same as was used in nonlinear baroclinic wave simulations by Simmons and Hoskins (1978). The value of K' is 2.338×10^{16} m^4 s^{-1}. From the smoothness of the results we present it is clear that this diffusion handles the cascade in the region of the critical line, but it is open to question whether it will represents the processes occurring in such a region. We use the values of the earth radius $a_0=6.371\times10^6$ m and rotation $\Omega=7.292\times10^{-5}$ s^{-1}. Considering the dominant external mode response, we choose the mean height of the free surface to be 10 km.

The solution of the perturbation problem has been checked by using an independently coded time-dependent shallow water equation model for which integrations have been described in Hoskins (1973).

b. Model zonal flows

The following six zonal flows were used for the calculations presented herein:

1. Super-rotation (i.e. constant angular velocity flow) with zonal velocity $\sim$15 m sec^{-1} at the equator, hereinafter referred to as SR.
2. 300 mb December–February observed mean zonal winds, D3.
3. 300 mb June–August observed mean zonal winds, J3.
4. 500 mb December–February observed mean zonal winds, D5.
5. 500 mb June–August observed mean zonal winds, J5.
6. Modification of D3 with no tropical easterlies, D3M.

The SR zonal flow has approximately the same angular momentum as D3. It has stationary wavenumber 7.5 implying that Rossby-Haurwitz waves of total wavenumber[2] 7 or smaller move westward relative to the underlying surface and those of total wavenumber 8 or larger move eastward.

The observed flows are taken from Oort and Rasmussen (1971) and Newell *et al.* (1969). Profiles of zonal flows 1–5 are presented in Fig. 1. The object of using these different flows is to test the sensitivity of our results. No implication is intended that the shallow water equations are more applicable to one level than another.

c. Model orography

1) SIMPLE ISOLATED MOUNTAINS

We have chosen the center of the mountain to be at $\lambda=180°$. Measuring the colatitude δ from the center of the mountain taken as pole, we define a circular mountain by $\phi^*=A(1+\cos W\delta)$ for $0\leqslant\delta\leqslant\pi/W$ and $\phi^*=0$, otherwise. Here, we select $W=8$ so that the diameter of the mountain is 45° latitude ($\sim$5000 km), and choose A such that the height of the center of the mountain is 2500 m. We also consider mountains whose projections on the tangent plane are elliptical with eccentricity $\epsilon=0.5$ referring to a mountain elongated in the east–west direction and shortened in the north–south direction, and with $\epsilon=2$ referring to a mountain elongated in the north–south direction.

2) EARTH OROGRAPHY

The basic earth topography was taken from the 1° grid values given by Gates and Nelson (1975). Using a least-squares method, a rhomboidal wavenumber 32 spectral analysis was obtained. This was then smoothed by multiplying the coefficients by $\exp[-kn^2(n+1)^2]$ with $k=\frac{1}{2}(\ln 10)/(42^2\times43^2)$, where n is the degree of the spherical harmonic. This gives multiplication factors 0.996, 0.675 and 0.003 for $n=10$, 32 and 63, respectively. The smoothed orography is shown in Fig. 2.

[2] The total wavenumber is the degree n of the corresponding spherical harmonic Y_n^m.

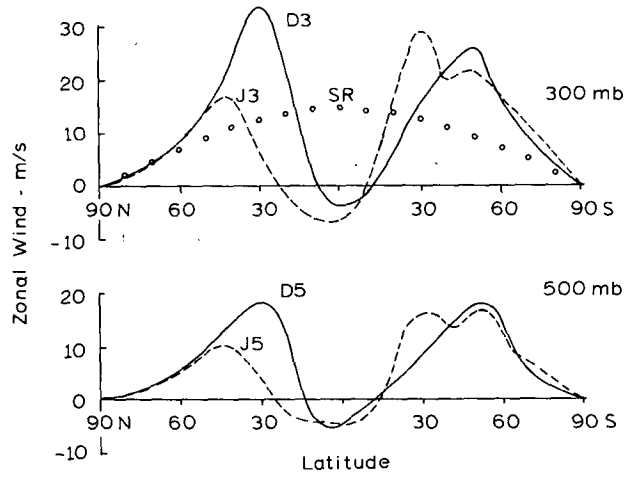

FIG. 1. The model zonal flows referred to in the text.

3. Solutions for simple orography

a. The use of wave propagation ideas

To establish an analogy with the study presented in H, we consider the following simplifications to (10) and (12). Scaling arguments suggest that to a good approximation, the variation in height of the free surface may be neglected in (12) which can be written

$$\nabla^2\alpha'=\frac{1}{\Phi}\frac{\bar{U}}{1-\mu^2}\frac{\partial\phi^*}{\partial\lambda}, \tag{13}$$

a form equivalent to that used by Charney and Eliassen (1949) and Bolin (1950). One of the experiments described below (D3 zonal flow with earth orography) was repeated using this approximation, and its validity was confirmed. Except for topography of global scale, the first term containing α' in the vorticity equation (10) may be neglected. Combining the result with (13) yields

$$\frac{\bar{U}}{1-\mu^2}\frac{\partial\xi'}{\partial\lambda}+\frac{\partial\psi'}{\partial\lambda}\frac{\partial\bar{\xi}}{\partial\mu}=-\frac{\bar{\xi}\bar{U}}{1-\mu^2}\frac{1}{\Phi}\frac{\partial\phi^*}{\partial\lambda}. \tag{14}$$

This is the steady barotropic vorticity equation with a forcing term due to orography. Anticyclonic vorticity is forced over the upslope region and cyclonic vorticity over the downslope. In H the time-dependent version of the barotropic vorticity equation was studied for simple localized forcing of one sign, and the development of wavetrains was exhibited. Here we will present results due to orographic forcing which may be understood as the superposition of the responses to negative

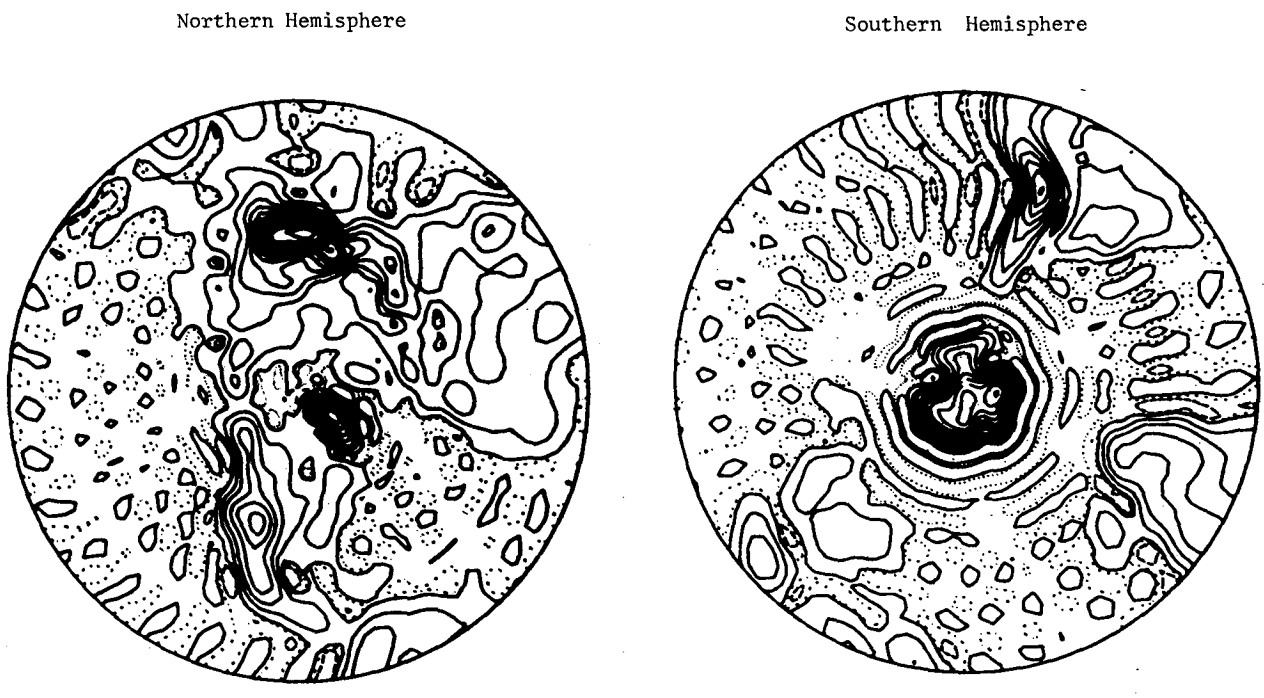

FIG. 2. The model earth orography shown in polar stereographic projections. The orography is obtained by smoothing a spectral expansion of the 1° grid values given by Gates and Nelson (1975). Positive contours are drawn at 10, 200 and 500 m, and then every 500 up to 5000 m. The spurious −10 m contour is dotted and −50 and −200 m contours are dashed. This negative value is exceeded only off the coast of South America where −467 m is attained. Longitudes 0° and 180° are indicated.

forcing on the upslope and to positive forcing on the downslope.

b. Super-rotation with a mountain at 30°N.

The flow pattern generated by the SR zonal flow over a mountain at 30°N is shown in Fig. 3. Presented on latitude-longitude grids are contours of perturbation vorticity ξ', total streamfunction $\psi=\bar{\psi}+\psi'$, and perturbation height field ϕ'. The ξ' field clearly shows a weak anticyclone upslope of and over the mountain, a downslope cyclone, and a train of waves downstream of the mountain. The wavetrain shows a tendency to split into a double structure in latitude. It exhibits strong northeast-southwest tilting and equatorial propagation, crossing to the antipodean region and then equatorward again. This far downstream, the amplitude of the disturbance is small and nearly dissipated before returning to the source, thereby avoiding resonance. The ψ field shows the same features but emphasizes the region of intensified winds southeast of the first trough downstream of the mountain, as was found by Bolin (1950). Because of the lack of amplitude in the equatorial regions, the perturbation height field ϕ', gives a suggestion of separate wavetrains in the two hemispheres and does not indicate the true propagation. Thus, in our subsequent descriptions we will consider only vorticity and streamfunction.

In H it was shown how the energy from a simple vorticity source of one sign propagated eastward and across the equator for this SR zonal flow. The above results are easily understood as the superposition of the wavetrains from the upslope and downslope regions.

The results for the elliptical mountains are quite similar. The elliptical mountain ($\epsilon=2$) elongated in the north–south direction exhibits no double structure in latitude. For the mountain elongated in the east–west direction ($\epsilon=0.5$), the wavetrain exhibits splitting after the downstream vorticity maximum, the next cyclonic center being north of 60°N. However, the energy then propagates into the Southern Hemisphere (SH) very much as for the circular mountain case. The shorter meridional scales in the $\epsilon=0.5$ mountain, as expected from H, lead to more north–south propagation from the sources.

c. Climatological zonal flows with a circular mountain at 30°N

When the circular mountain at 30°N perturbs the D3 zonal flow, the major difference from the SR results is the absence of any nonzero contours in ξ' in the SH south of 5°S. Use of the zonal flow D3M with 4 m s^{-1} tropical westerlies, however, allows propagation into the SH with magnitudes of ξ' not much less than for the SR flow. Thus, equatorial easterlies provide an effective barrier for stationary waves.

The Northern Hemisphere response (NH) for flow D3 is shown on a polar sterographic map projection in Fig. 4a. There is a similarity to the SR results with an

upslope anticyclone, downslope cyclone and a downstream system of waves. The vorticity field now shows a definite split in the wavetrain, with northern extrema poleward of 60°N and larger southern extrema near 20°N with very strong northeast-southwest tilting on the equatorial side. The dividing line between the two wavetrains is about 42°N. To the north of this line the dominant zonal wavelength corresponds to about

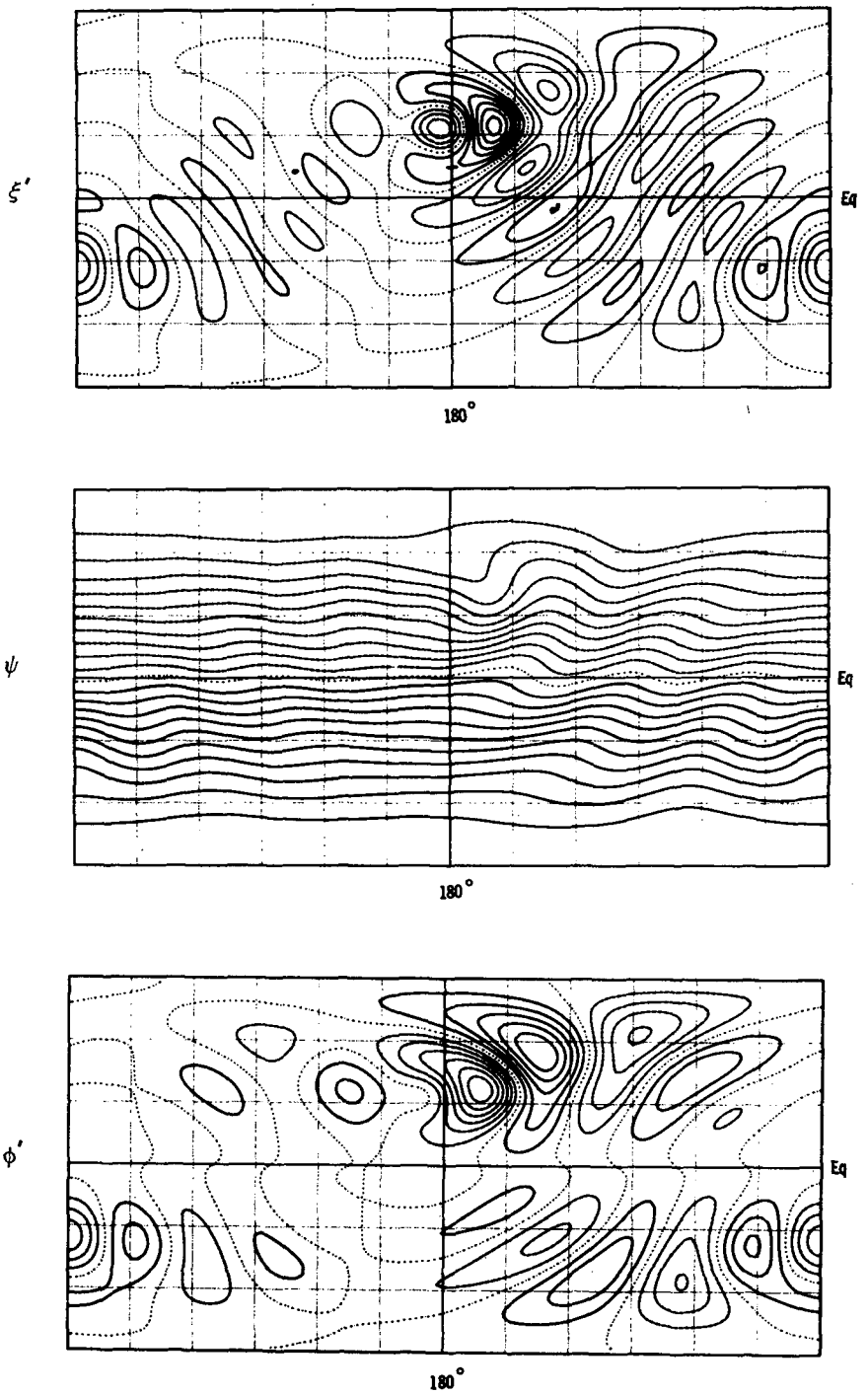

FIG. 3. Super-rotation zonal flow with a circular mountain at 30°N. On latitude-longitude maps are shown contours of (a) the perturbation vorticity field ξ', (b) the total streamfunction ψ, (c) the perturbation height field, ϕ'. Lines of latitude and longitude are drawn every 30°. Zero contours are dotted and negative contours dashed. At longitude 180° the mountain extends from 7.5°S to 52.5°N.

wavenumber 3 and to the south about wavenumber 5. This point will be discussed further in Section 5. The strong tilts equatorward of 15°N are consistent with the expected behavior in this region where there are westerlies to the north and easterlies to the south (see, e.g., H).

The ψ field in Fig. 4a shows a strongly tilted trough centered about 20° downstream from the mountain. Again there is strong flow on the southeast flank between the positive vorticity perturbation to the northwest and the anticyclone to the southeast. Associated with the latter are the strongest equatorial easterlies, about 40° downstream from the mountain. About 80° downstream there is a ridge to the north and a trough to the south associated with the different phases of the two wavetrains. There is a weaker, untilted trough about 150° downstream where the two wavetrains are again in phase. The ridge slightly upstream of the mountain is only a weak feature.

The height field perturbation (not shown) is smoother than ξ' with the strongly tilted pattern equatorward of 20°N missing and the amplitudes in the northern train of waves larger than those in the subtropical train.

The corresponding ξ' and ψ fields for zoal flows D5 and J3 are shown in Figs. 4b and 4c. The results for the case with zonal flow D5 are quite similar to those for D3. There is splitting of the wavetrain, with the northern portion exhibiting larger amplitudes than with D3. The largest difference is in the wavelengths produced. The downslope trough is again about 20° downstream, but the "blocking" region is about 60° and the untilted trough about 100° downstream. The center of the enhanced equatorial easterlies is about 30° downstream. These shorter length scales are to be expected for this weaker zonal flow. The J3 solution exhibits a weaker wavetrain whose equatorial portion is absent due to the easterly winds equatorward of 23°N. There is an indication of a minimum in the vorticity amplitude near 55°N with smaller zonal wavenumbers dominant to the north. The ψ field shows a tilted downstream trough, ridge and trough about 15°, 50° and 80° downstream. The J5 flow (not shown) gives a similar, but still weaker response.

d. Circular mountain at other latitudes

Perturbing the zonal flows with a circular mountain at 60°N yields a large vorticity response near the mountain and a strongly east-northeast to south-southwest tilted wavetrain. The waves display no splitting tendency.

As a simple model of Antarctica, we center the mountain at 80°S so that it extends from 57.5°S on the 180° longitude over the pole to 77.5°S on the 0° longitude. The zonal flows SR and D3 have been used, giving qualitatively similar results. The result for the D3 zonal flow in the SH is shown in Fig. 5. We observe anticyclonic (positive in SH) vorticity forced on the upslope and cyclonic (negative in SH) vorticity on the downslope. The ξ' field shows a dominant zonal wavenumber 1 with large amplitude near the pole and weak spirals radiating outward. Taking account of the change in hemisphere, the picture is similar to that obtained with the mountain at 60°N, but with even larger tilts. The ψ field shows the downslope trough situated some 110° downstream of the mountain center. The upslope, ridge is about 20° upstream. With the SR zonal flow the forcing is approximately half as large and so is the response. Otherwise, the main difference is the phase of the pattern. The downslope trough, for instance, is approximately 40° nearer the mountain.

4. Solutions for earth orography

The simple experiments described in the previous section give us the basis for understanding the steady

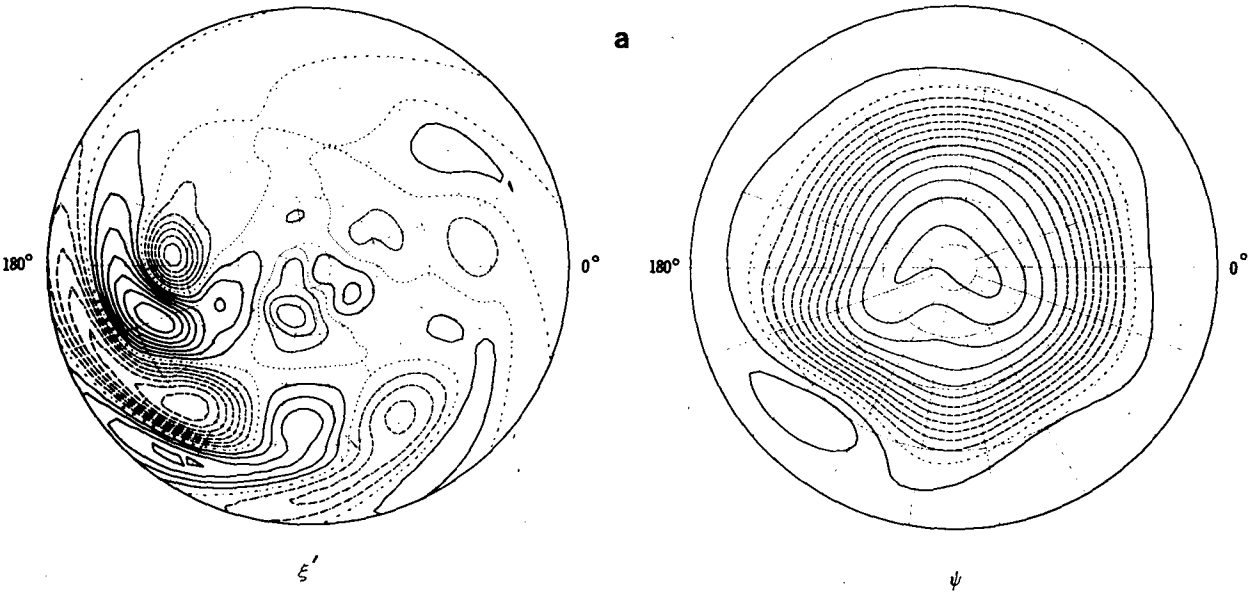

ξ' ψ

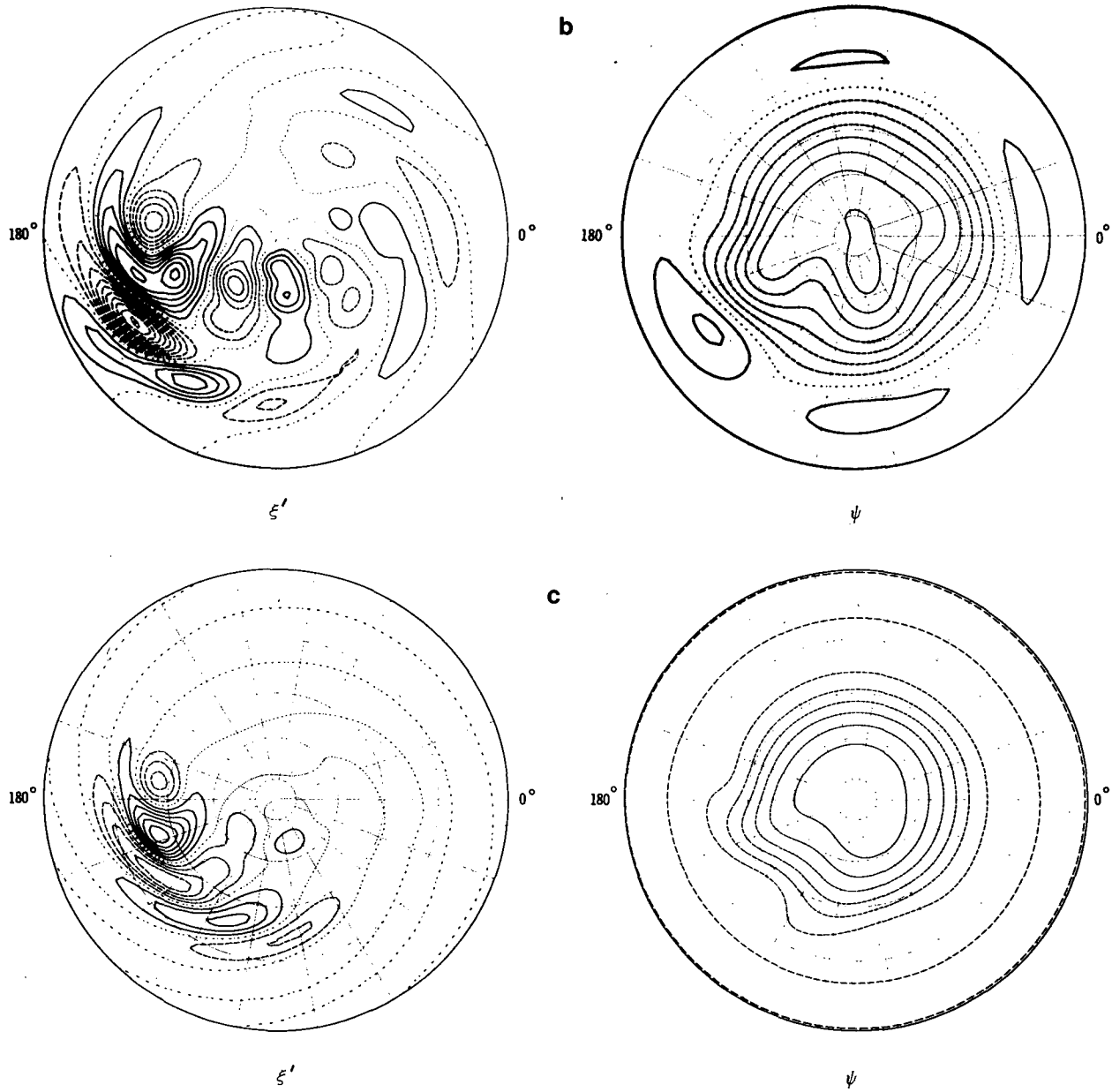

FIG. 4. Climatological zonal flows with a circular mountain at 30°N. The zonal flows are (a) D3, (b) D5, (c) J3. The plots are Northern Hemisphere polar stereographic projections with lines of latitude and longitude drawn every 20°. In each case the mountain is centered about 180° longitude. The perturbation vorticity ξ' is on the left and total streamfunction ψ on the right. Zero contours are dotted and negative contours dashed.

response to the more complicated orography of the earth as described by the linearized, shallow water equations. The smoothed orography used is that previously referred to in Fig. 2. The results for the D3 zonal flow using that orography are shown in Fig. 6. Considering the SH first, comparison with Fig. 5 shows that the response is mostly well described as that due to a circular mountain off-centered from the pole at about 70°E. The other features which are noticeable, particularly in ξ', are the downstream, equatorward trough and ridge from the Andes, and a smaller perturbation by Southern Africa. The NH maps are due mainly to the influence of the Himalayas, the Rocky Mountains and Greenland. In some places the wavetrains from the different sources tend to reinforce and in other places they tend to interfere. The Himalayas act very much like the 30°N circular mountain in Fig. 4a. They produce a lee trough over Eastern Asia and a split wavetrain. The equatorward train produces intense flow to the southeast of the trough and significant equatorial easterlies near 140°E. The northern train produces the Aleutian ridge and aids the formation

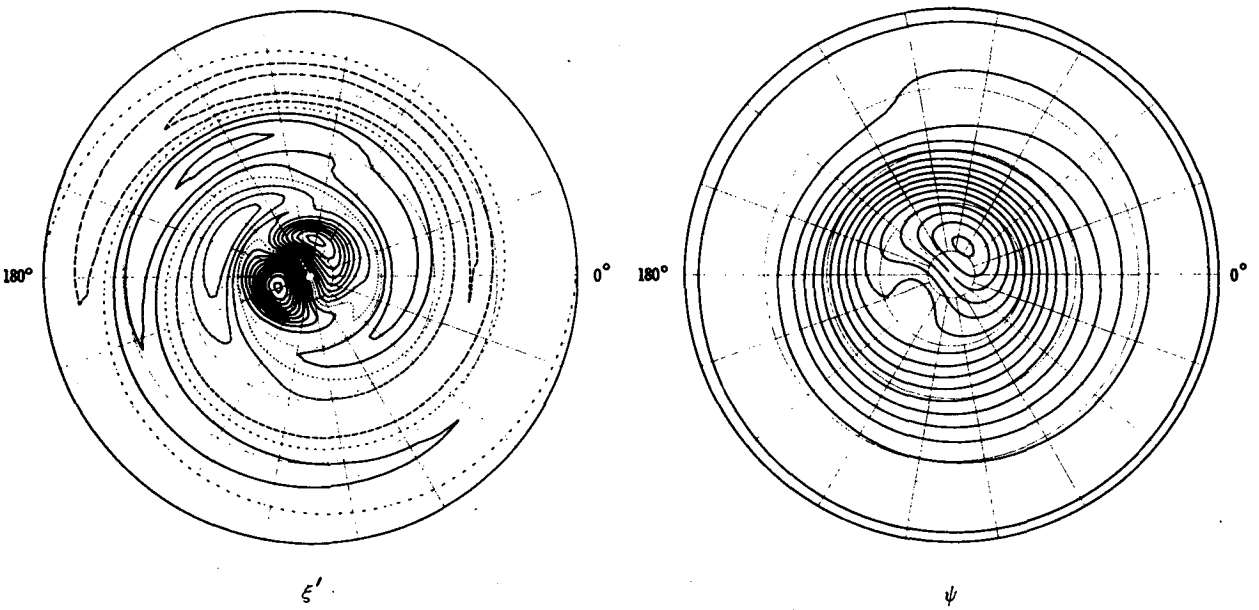

FIG. 5. Zonal flow D3 with mountain at 80°S. The plots are Southern Hemisphere polar stereographic projections. Plotting conventions as in Fig. 4.

of a trough over the Hudson Bay. The orographic forcing due to the Rockies tends to have a double maximum associated with the peaks at 60 and 40°N. The upslope associated with the northern maximum reinforces the Aleutian ridge and the downslope the Hudson bay trough. The southern upslope ridge is weak and the southern train of waves, though significant, suffers from some interference between the upslope and downslope sources due to the confined longitudinal scale. The northern train of waves is in phase with the upslope ridge due to Greenland. The Greenland downslope cyclonic maximum is centered near 35°E and the almost equatorward wavetrain expected on the basis of the results in Section 3b appears as a westward extension to 20°E of the Himalayan waves. The ψ field shows the same ridge and trough features. It emphasizes the strong westerly and easterly winds off the east coast of Asia and the diffluence of the flows in the Pacific and Atlantic.

The D5, J3 and J5 zonal flows have also been used with the earth orography. The SH maps are not shown because the results are very similar to those shown above. However, it may be noted that the off-pole vortex is moved 20°–30° upstream for the weaker 500 mb flows. The NH maps for D5 are shown in Fig. 7a. The ξ' fields show the same propagation features as discussed above, although with the weaker flows and consequently smaller scale response, there is less interference between the influence of different mountain complexes. Zonal flow D5 produces a larger southern response to the Rockies, the weaker flow fitting in better with the scale of the mountains. The northern train from the Hamalayas with its smaller scale produces an extra trough in the Aleutian region and reinforces a larger upslope anticyclone over the west coast of North America. The corresponding ψ field shows a four trough pattern with the Pacific flow modified to a "blocking" pattern in the west, a trough in the center, and a ridge to the east.

As found in the simple experiments, the summer flows (J3 and J5) do not show the same strong tendency for producing split wavetrains. The results for the J3 flow (Fig. 7b) show almost separate wavetrains from each mountain complex. There is still a slight ridge north of a trough at 20°W, but this is associated mainly with the Greenland upslope response north of the wavetrain from the Rockies. The streamfunction pattern shows three troughs at 60°N and seven at 35°N, all considerably weaker than for the winter flows. The J5 response (not shown) is very similar but considerably weaker.

5. Discussion

The intention in this paper has not been to give a definitive account of the effects of large-scale orographic forcing, but to provide suggestive material on the possible regions and forms of influence of mountains, and to provide some insight into the features to be looked for in more complicated models. However, it is clearly of interest to compare our results with observed seasonally averaged fields.

The wave pattern with the D3 zonal flow is surprisingly realistic. The NH troughs and ridges at 60°N are in almost the observed positions of 35°E, 135°E and 80°W. The seasonally averaged equatorial winds shown by Newell *et al.* (1972) have maximum easterlies near 150°E, an isolated easterly maximum near 70°W

and strongest westerlies at about 35°W, also consistent with our results. On the other hand, the observed SH trough in wavenumber 1 at 60°S is near 120°W, in disagreement with Fig. 6b. The weaker D5 zonal flow gave a NH result which was similar though less realistic in the Pacific. The fact that the shallow water equations when linearized about the observed 300 mb zonal flow and perturbed only by the earth orography give a NH wave pattern as realistic as can be produced by almost any model is certainly worthy of note. It suggests that insights gained from our simple model are useful and worthy of investigation in more complicated models.

One feature which is of particular interest is the split wavetrains produced by midlatitude mountains in the winter zonal flows. This is the object of current study using ray tracing techniques. Some understanding of this splitting may be obtained by considering the nondimensional bartropic vorticity equation on a Mercator projection of the sphere:

$$\left(\frac{\partial}{\partial t}+\bar{u}\frac{\partial}{\partial x}\right)(\psi_{xx}+\psi_{yy})+\tilde{\beta}\psi_x=0, \tag{15}$$

where $x=\lambda$ and $y=\tanh^{-1}(\sin\theta)$ and

$$\tilde{\beta}=2\cos^2\theta-\cos\theta\frac{\partial}{\partial\theta}\left[\frac{1}{\cos\theta}\frac{\partial}{\partial\theta}(\bar{u}\cos^2\theta)\right], \tag{16}$$

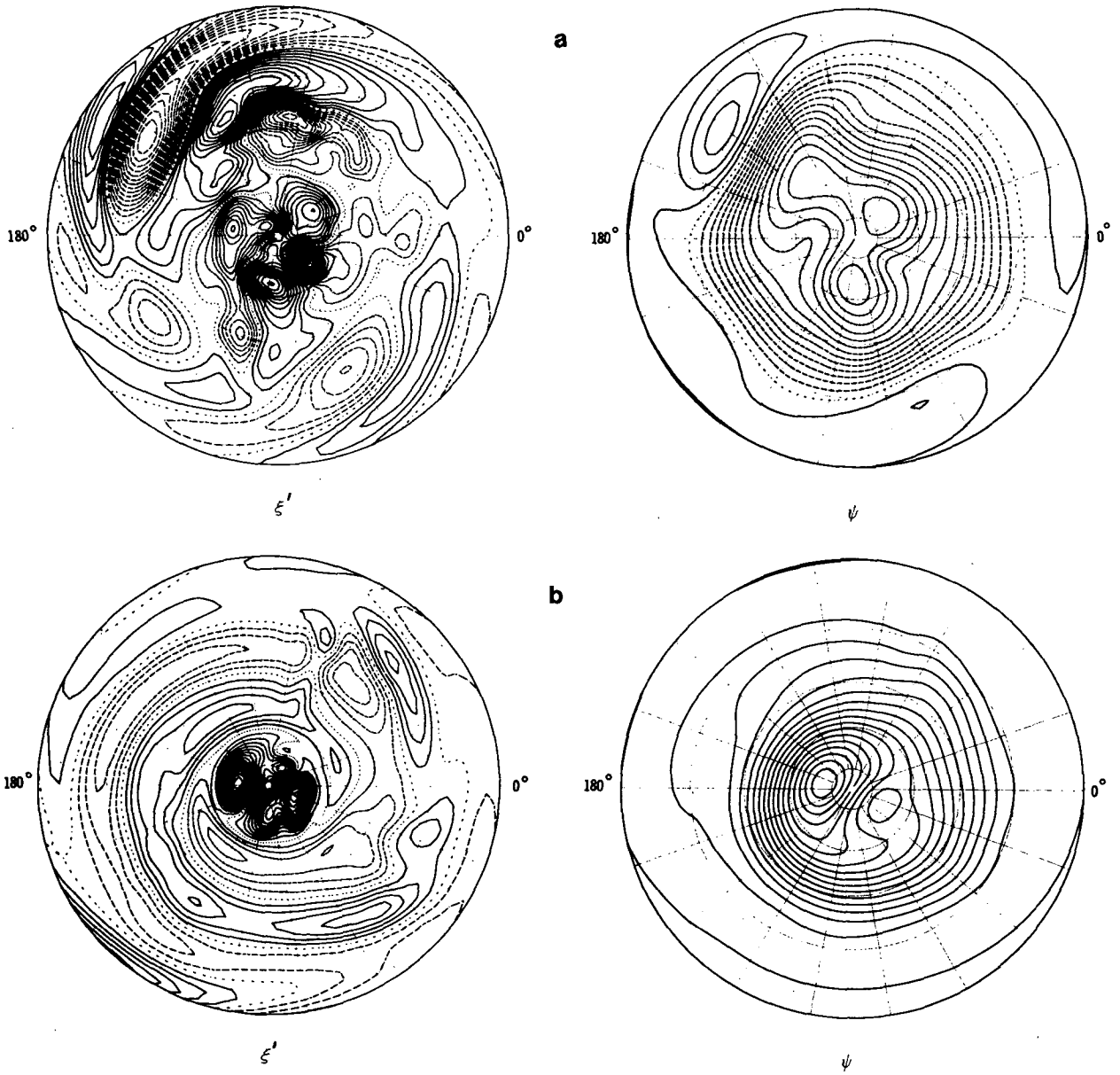

FIG. 6. Zonal flow D3 with earth orography, showing vorticity perturbation ξ' and total streamfunction ψ: (a) Northern Hemisphere, (b) Southern Hemisphere. Plotting conventions as in Fig. 4.

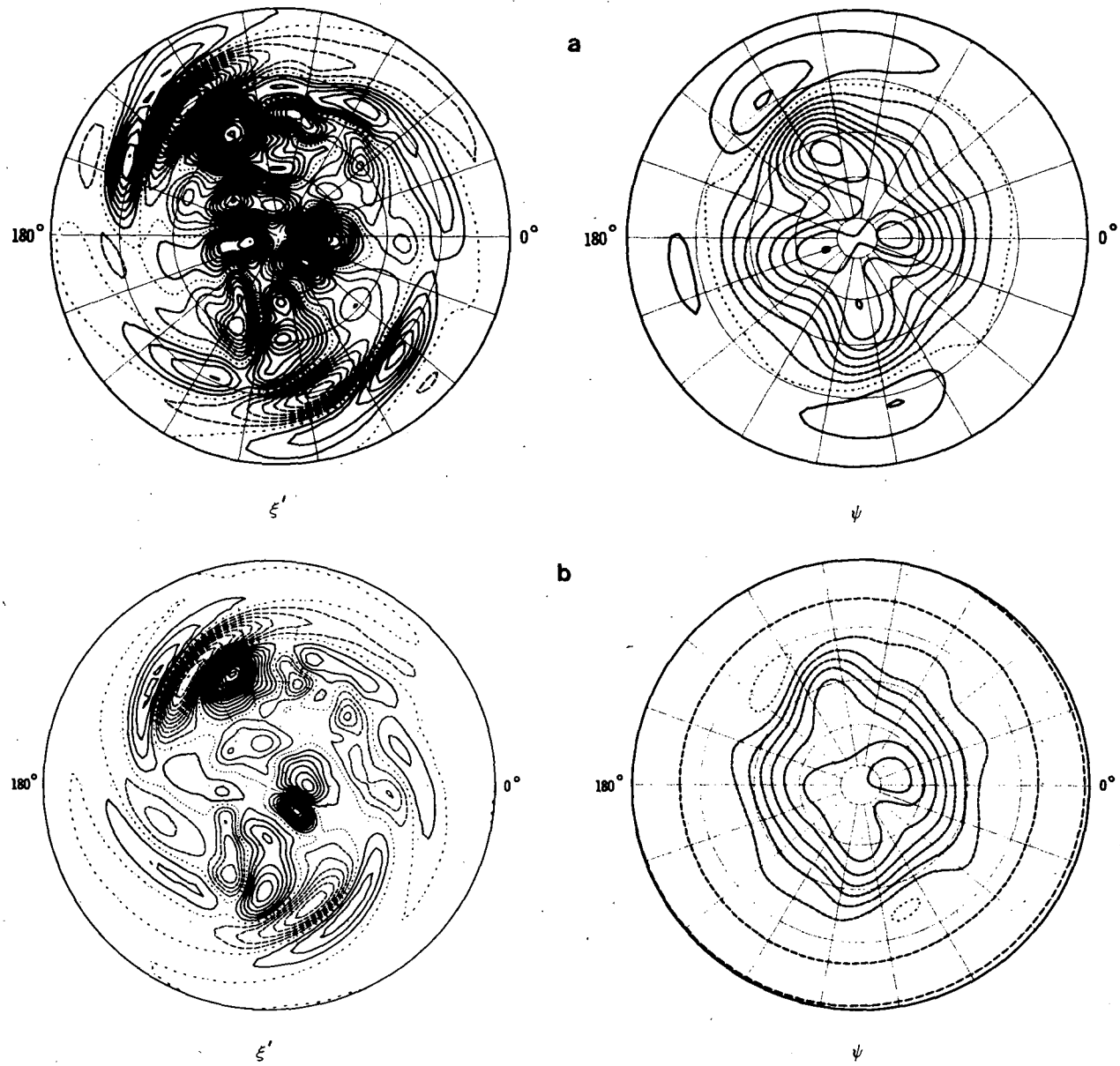

FIG. 7. Northern Hemisphere plots of perturbation vorticity ξ' and total streamfunction ψ for earth orography in zonal flow (a) D5, (b) J3. Plotting conventions as in Fig. 4.

and $\bar{u}=\tilde{U}/\cos^2\theta$ is proportional to the angular velocity. Assuming that zonal flow properties vary sufficiently slowly in latitude, we may look for a local solution of the form $\exp i(kx+ly)$. We may then define a local stationary wavenumber as the value of the total wavenumber $(k^2+l^2)^{\frac{1}{2}}$ which gives zero rate of change

$$K_s=\left(\frac{\tilde{\beta}}{\bar{u}}\right)^{\frac{1}{2}}. \tag{17}$$

For a super-rotation $\bar{u}=\epsilon$

$$K_s=[2(1+\epsilon^{-1})]^{\frac{1}{2}}\cos\theta, \tag{18}$$

which varies smoothly from zero at the pole to approximately 8 at the equator for the SR flow. This result is consistent with the SR solution in Fig. 3 in which there is a smooth transition from long wavelengths near the pole to short wavelengths near the equator. When the zonal flow contains a strong jet, the local stationary wavenumber tends to show a jump on the poleward flank of the jet. For the D3 zonal flow K_s is shown in Fig. 8. From 70 to 40°N K_s lies between 3 and 4 and from 35 to 15°N between 5 and 7.2. The actual local zonal wavenumber in the wavetrain generated by the circular mountain in this flow (Fig. 4a) has been estimated and is also shown in Fig. 8. Clearly the split wavetrain and longer wavelengths in the poleward

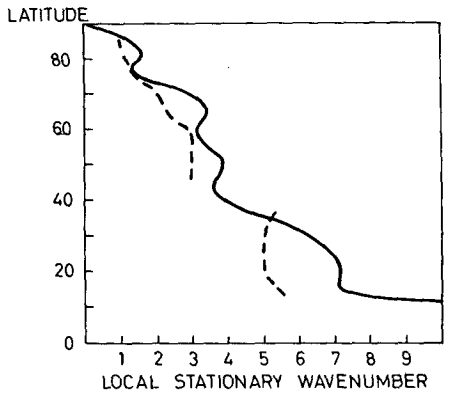

FIG. 8. The local stationary wavenumber, as defined in the text, for the Northern Hemisphere of the D3 zonal flow. Indicated by a dashed line is the local zonal wavenumber (estimated) from Fig. 4a.

train are consistent with the local stationary wavenumber analysis.

To highlight the importance of equatorial easterlies in isolating the standing waves in the two hemispheres, the SH streamfunction for the earth orography in the D3M zonal flow is shown in Fig. 9. The only difference from D3 is that the equatorial flow is 4 m sec^{-1} westerly, but the contrast with Fig. 6b is striking.

In this paper, by linearizing about a zonal flow, we have tacitly assumed that orographic forcing is well represented by demanding that air flow be over and not around mountains. This assumption may be particularly poor for Antarctica where only small meridional motion could drastically change the uplifting of the flow. However, discussion of such nonlinearities is beyond the scope of this present paper.

The results described here emphasize the two-dimensional nature of the horizontal wave propagation on the sphere and the necessity for quantitative theories of the stationary waves to contain a full representation of the spherical domain. In contrast, Charney and Eliassen (1949) used a β plane with trivial y variation and both Kasahara (1966) and Derome and Wiin-Nielsen (1971) also adopted the β plane approximation. Bolin (1950) did allow some variation of β with latitude in his circular mountain solution and consequently obtained the preferred northeast-southwest tilt of the troughs. Egger (1976a) included the full spherical geometry, but this resolution of 7.5° in latitude and eight zonal waves was insufficient for study of the wavetrains in his solutions.

FIG. 9. Zonal flow D3M with earth orography showing total streamfunction for the Southern Hemisphere.

Acknowledgments. The authors are grateful to Adrian Simmons, David Andrews, Richard Lindzen and David Karoly for helpful discussions on the work presented here. One of the authors (WLG) is particularly appreciative to Professor Robert P. Pearce and the University of Reading for permitting him to pursue a period of study and research with the United Kingdom Universities' Atmospheric Modeling Group.

APPENDIX

Method of Solution

The dependent variables ψ', α', ϕ' and the orography ϕ^* are expressed as truncated series of spherical harmonics

$$X' = \sum_{m=-M}^{M} \sum_{n=|m|}^{|m|+J} X_n^m P_n^m(\mu) e^{im\lambda},$$

where X' stands for ψ', α', ϕ' or ϕ^* and P_n^m are the associated Legendre functions. A rhomboidal truncation with $M=32$ and $J=31$ has been used. Substitution into the perturbation equations (10)–(12), multiplication by $P_l^m e^{-im\lambda}$ and integration over the sphere yields independent sets of linear equations for each zonal wavenumber m. For each m these may be written in the easily soluble form

$$\begin{bmatrix} \mathbf{G1} & \mathbf{G2} & 0 \\ \mathbf{H1} & \mathbf{H2} & \mathbf{H3} \\ \mathbf{J1} & \mathbf{J2} & \mathbf{J3} \end{bmatrix} \begin{bmatrix} \boldsymbol{\psi} \\ \boldsymbol{\alpha} \\ \boldsymbol{\phi} \end{bmatrix} = \begin{bmatrix} 0 \\ 0 \\ \mathbf{S} \end{bmatrix},$$

where $\boldsymbol{\psi}$, $\boldsymbol{\alpha}$, $\boldsymbol{\phi}$ are the column vectors $(\psi_m^m, \psi_{m+1}^m, \ldots)$, etc., and

$$\begin{aligned} G1_{ln} &= -mc_n F1_{ln} + mF5_{ln}, \\ G2_{ln} &= F6_{ln} - C_n F3_{ln}, \\ H1_{ln} &= -C_n F2_{ln} - F6_{ln} + C_n F4_{ln} + C_l F2_{ln}, \\ H2_{ln} &= -mF5_{ln} + mC_l F1_{ln}, \\ H3_{ln} &= -C_l \delta_{ln}, \\ J1_{ln} &= mF7_{ln}, \\ J2_{ln} &= F8_{ln} - C_n F9_{ln}, \\ J3_{ln} &= mF1_{ln}, \\ S_l &= m \sum_n F1_{ln} \phi^{*m}_n, \end{aligned}$$

where $C_n=n(n+1)$ and the zonal integrals are

$$F1_{ln}=\int_{-1}^{1}\frac{\bar{U}}{1-\mu^2}P_nP_l d\mu,$$

$$F2_{ln}=\int_{-1}^{1}\bar{U}\frac{dP_n}{d\mu}P_l d\mu,$$

$$F3_{ln}=\int_{-1}^{1}\bar{\xi}P_nP_l d\mu,$$

$$F4_{ln}=\int_{-1}^{1}\left(\bar{\xi}-\frac{d\bar{U}}{d\mu}\right)P_nP_l d\mu,$$

$$F5_{ln}=\int_{-1}^{1}\frac{d\bar{\xi}}{d\mu}P_nP_l d\mu,$$

$$F6_{ln}=\int_{-1}^{1}\frac{d\bar{\xi}}{d\mu}(1-\mu^2)\frac{dP_n}{d\mu}P_l d\mu,$$

$$F7_{ln}=\int_{-1}^{1}\frac{d\bar{\phi}}{d\mu}P_nP_l d\mu,$$

$$F8_{ln}=\int_{-1}^{1}\frac{d\phi}{d\mu}(1-\mu^2)\frac{dP_n}{d\mu}P_l d\mu,$$

$$F9_{ln}=\int_{-1}^{1}(\Phi+\bar{\phi})P_nP_l d\mu.$$

Note that in the above equations for the **F**, **G**, **H** and **J** matrices, the **S** vector and the Legendre functions P_n, the superscript m has been suppressed. When linear drag and biharmonic diffusion are added to the momentum equations, a term $i(Kc_l+K'C_l^3)\delta_{ln}$ must be added to $G1$ and subtracted from $H2$.

All of the above zonal flow integrals are polynomials of order less than or equal to $2M+3J$, and may therefore be evaluated exactly by Gaussian quadrature on at least $(2M+3J+1)/2$ or 79 Gaussian latitudinal points.

For the SR zonal flow, it is easily seen that

$$\bar{U}=\nu(1-\mu^2),$$
$$\bar{\xi}=2\mu(1+\nu),$$
$$\bar{\phi}=\nu(1+\tfrac{1}{2}\nu)(\tfrac{1}{3}-\mu^2),$$

and the integrals may be evaluated directly. For our studies, $\nu=0.0324$.

For the observed zonal flows, the vorticity coefficients are obtained from the observed wind U_0 at Gaussian latitudes using

$$\xi_n^0=\int_{-1}^{1}U_0\frac{dP_n^0}{d\mu}d\mu.$$

Then the model wind is

$$\bar{U}=(1-\mu^2)\sum_{n=0}^{J}\frac{\xi_n^0}{C_n}\frac{dP_n^0}{d\mu}$$

and the relative vorticity

$$-\frac{d\bar{U}}{d\mu}=\sum_{n=0}^{J}\xi_n^0P_n^0.$$

The variable $d\bar{\phi}/d\mu$ is given by (9). Using the recursion relation for $(1-\mu^2)\,dP_n^0/d\mu$ in terms of P_{n-1}^0 and P_{n+1}^0, the spectral coefficients $\bar{\phi}_n^0$ may be obtained sequentially and hence grid-point values of $\bar{\phi}$ obtained.

REFERENCES

Bolin, B., 1950: On the influence of the earth's orography on the general character of the westerlies. *Tellus*, **2**, 184–195.

Charney, J. G., and A. Eliassen, 1949: A numerical method for predicting the perturbations of the middle latitude westerlies. *Tellus*, **1**, 38–54.

Derome, J., and A. Wiin-Nielsen, 1971: The response of a middle-latitude model atmosphere to forcing by topography and stationary heat sources. *Mon. Wea. Rev.* **99**, 564–576.

Egger, J., 1976a: The linear response of a hemispheric two-level primitive equation model to forcing by topography. *Mon. Wea. Rev.*, **104**, 351–364.

——, 1976b: On the theory of the steady perturbations in the troposphere. *Tellus*, **28**, 381–389.

Gates, W. L., and A. B. Nelson, 1975: A new (revised) tabulation of the scripps topography on a one degree global grid. Part I: Terrain heights. The Rand Corporation, R-1276-1-ARPA, Santa Monica, CA.

Gilchrist, B., 1954: The seasonal phase changes of thermally produced perturbations in the westerlies. *Proc. Toronto Meteor. Conf.*, Amer. Meteor. Soc. and Roy. Meteor. Soc. 129–131.

Hoskins, B. J., 1973: Stability of the Rossby-Haurwitz wave. *Quart. J. Roy. Meteor. Soc.* **99**, 723–745.

——, A. J. Simmons and D. G. Andrews, 1977: Energy dispersion in a barotropic atmosphere. *Quart. J. Roy. Meteor. Soc.*, **103**, 553–567.

Kasahara, A., 1966: The dynamical influence of orography on the large-scale motion of the atmosphere. *J. Atmos. Sci.*, **23**, 259–271.

——, T. Sasamori and W. M. Washington, 1973: Simulation experimental with a 12-layer stratospheric global circulation model. I. Dynamical effect of the earth's orography and thermal influence of continentality. *J. Atmos. Sci.*, **30**, 1229–1251.

Manabe, S., and T. B. Terpstra, 1974: The effects of mountains on the general circulation of the atmosphere as identified by numerical experiments. *J. Atmos. Sci.*, **31**, 3–42.

Newell, R. E., D. G. Vincent, T. G. Dopplick, D. Ferruza and J. W. Kidson, 1969: The energy balance of the global atmosphere. *The Global Circulation of the Atmosphere*, G. A. Corby, Ed., Roy. Meteor. Soc., 42–90.

Oort, A. H., and E. M. Rasmusson, 1971: Atmospheric circulation statistics. NOAA Prof. Paper 5, Govt. Printing Office, Washington, DC. 323 pp.

Simmons, A. J., and B. J. Hoskins, 1978: The life cycles of some nonlinear baroclinic waves. *J. Atmos. Sci.*, **35**, 414–432.

Smagorinsky, J., 1953: The dynamical influence of large-scale heat sources and sinks on the quasi-stationary mean motions of the atmosphere. *Quart. J. Roy. Meteor. Soc.*, **79**, 342–366.